Numerical simulation of shock wave focusing at fold caustics, with application to sonic boom

Régis Marchiano[a] and François Coulouvrat
Laboratoire de Modélisation en Mécanique, UMR CNRS 7607, Université Pierre et Marie Curie, 8 rue du Capitaine Scott, 75015 Paris, France

Richard Grenon
Département d'Aérodynamique Appliquée, DAAP/ACI, ONERA, 29 Avenue de la division Leclerc, BP2, 92322 Châtillon Cedex, France

(Received 13 February 2003; revised 11 July 2003; accepted 28 July 2003)

Weak shock wave focusing at fold caustics is described by the mixed type elliptic/hyperbolic nonlinear Tricomi equation. This paper presents a new and original numerical method for solving this equation, using a potential formulation and an ''exact'' numerical solver for handling nonlinearities. Validation tests demonstrate quantitatively the efficiency of the algorithm, which is able to handle complex waveforms as may come out from ''optimized'' aircraft designed to minimize sonic booms. It provides a real alternative to the approximate method of the hodograph transform. This motivated the application to evaluate the ground track focusing of sonic boom for an accelerating aircraft, by coupling CFD Euler simulations performed around the mock-up on an adaptated mesh grid, atmospheric propagation modeling, and the Tricomi algorithm. The chosen configuration is the European Eurosup mock-up. Convergence of the focused boom at the ground level as a function of the matching distance is investigated to demonstrate the efficiency of the numerical process. As a conclusion, it is indicated how the present work may pave the way towards a study on sonic superboom (focused boom) mitigation. © *2003 Acoustical Society of America.*
[DOI: 10.1121/1.1610459]

PACS numbers: 43.25.Cb, 43.25.Jh [MFH]

I. INTRODUCTION

Sonic booms remain a community acceptance problem that may jeopardize the development of future civil supersonic aircraft (either supersonic transport or business jet). The most intense sonic boom is the focused sonic boom due to the aircraft transonic acceleration from Mach 1 to cruise speed, and it cannot be avoided by realistic maneuvers. It leads to an amplification of ground pressures up to two to three times the carpet boom shock strength. Therefore, to comply with a future international regulation on sonic boom, it is important to predict accurately the level of focused booms. The present work will demonstrate such a prediction is now within reach. It is a complex task, as it requires a precise CFD simulation of the pressure field far enough from the aircraft, a correct matching between aerodynamical evaluations and acoustical propagation modeling in the atmosphere, and a validated modeling of shock waves focusing around the caustic at ground level.

According to the classic theory (Hayes *et al.*, 1969), sonic booms are computed within the framework of geometrical acoustics. The eikonal (phase) function is determined by the ray path, and the signal amplitude by the ray-tube area. Nonlinear effects along each ray entail the pressure signal to evolve from the complicated shock flow around the body of the aircraft down to the ultimate ''N'' wave reached at ground level for long propagation distances. The input pressure signal describing the aircraft flow field was initially estimated from the linear aerodynamic theory for slender bodies (Whitham, 1952), a theory that also provides the correct matching to geometrical acoustics. However, Whitham's linear approximation lacks precision for relatively low Mach numbers such as those of acceleration focusing (around Mach 1.2 to 1.4). Nowadays numerical means enable CFD simulations to be reliable far enough from the aircraft (one or several fuselage lengths). Direct matching between CFD simulations and acoustical propagation can be achieved for cruise (steady) flight, with a good convergence at ground level provided the matching is performed far enough from the aircraft. More sophisticated ways of matching can be achieved closer to the aircraft, but have not been fully explored yet (Plotkin and Page, 2002).

Caustics are surfaces, and their ground intersection are lines, where the ray-tube area vanishes and the geometrical acoustics approximation neglecting diffraction breaks down. Around regular smooth caustics surfaces [''fold'' caustics according to the terminology of catastrophe theory (Thom, 1972; Berry, 1976)], diffraction must be taken into account inside a ''diffraction boundary layer'' around the caustic (Buchal and Keller, 1960) to be matched to geometrical acoustics. Within this layer, the pressure satisfies the linear Tricomi equation, whose generic solution in the frequency domain is the well-known Airy function, in agreement with the catastrophe theory. If, as for sonic booms, the incoming signal possesses shock waves, the amplified signal near the caustics and the outgoing signal exhibit a ''U'' shape resulting from the $\pi/2$ phase jump through the caustics. This shape is substantiated by flight tests (Wanner *et al.*, 1972), but the

[a]Electronic mail: marchi@lmm.jussieu.fr

 0001-4966/2003/114(4)/1758/14/$19.00

linear theory fails to predict finite peaks for the ''U'' wave. To recover finite amplitudes, nonlinearities must be taken into account as an additional ''limiting'' mechanism. The resulting equation satisfied by the pressure field is the so-called *nonlinear Tricomi equation* (Guiraud, 1965) which is a mixed-type (elliptic/hyperbolic) equation (Sec. II). The process of linear diffraction being the dominant mechanism around caustics, supplemented by nonlinearities, is supported by laboratory-scale experiments (Sturtevant and Kulkarny, 1976; Marchiano *et al.*, 2003) at small Mach numbers. The objective of this paper is to present a new numerical method to solve the *nonlinear Tricomi equation* using a pseudospectral method, and to apply it for predicting ground track sonic boom focusing coupled with CFD nearfield simulations of a realistic high-speed supersonic transport.

The new algorithm for solving the nonlinear Tricomi equation derives from a previous version (Auger and Coulouvrat, 2002). The reader is referred to this work for an extensive bibliography on numerical methods applied to the nonlinear Tricomi equation. Let us only cite the most recent work of Cheng and Hafez (2002). Compared to this previous code, two very substantial improvements have been brought (Sec. III). The equation is now solved for the potential field instead of the pressure field, and nonlinear effects are treated with an ''exact'' solver that removes artificial numerical dissipation and avoids any stability condition. This results into an innovative combination of numerical methods with potential applications for other equations in nonlinear acoustics (such as the KZ equation). As a consequence, the number of iterations and the computation time have been reduced dramatically by a factor of (roughly) 40, the convergence of the maximum peak amplitude with mesh refinement is now perfectly reached, and the theoretical Guiraud's similitude is satisfied numerically with a good precision. This constitutes a complete and quantitative validation of the algorithm (Sec. IV), which is able to handle complex waveforms as may come out from ''optimized'' aircraft designed to minimize sonic booms. It provides a real alternative to the approximate method of the hodograph transform developed by Seebass (1971) and Gill and Seebass (1973), and currently applied for the numerical evaluation of the superboom (Plotkin, 2002). This motivated the application to evaluate the ground track focusing of the sonic boom of an accelerating aircraft, by coupling CFD Euler simulations performed far away from the aircraft on an adaptated mesh grid, atmospheric propagation modeling, and the Tricomi algorithm (Sec. V). Convergence of the focused boom at ground level as a function of the matching distance is investigated to demonstrate the efficiency of the numerical process. As a conclusion, we indicate how the present work may pave the way towards a study on sonic superboom (focused boom) mitigation.

II. THE PHYSICAL PROBLEM: THE NONLINEAR TRICOMI EQUATION

From a physical point of view, a caustic is a region where sound is amplified. In terms of geometrical acoustics, it is the locus of points where the ray-tube area vanishes and where the geometrical approximation breaks down. It is also an envelope of rays, tangent to acoustical rays at any point.

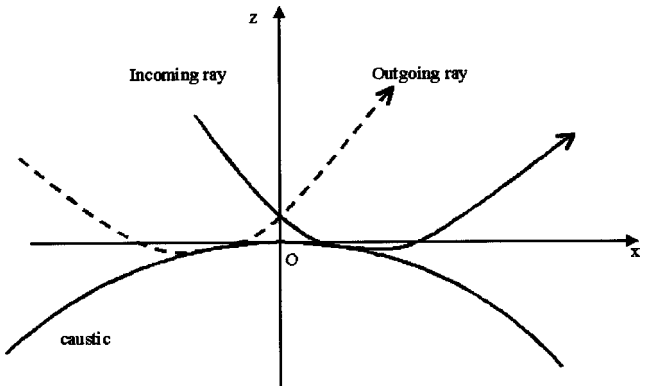

FIG. 1. Geometry of the caustic.

So, near a regular caustic [a fold caustic in the terminology of catastrophe theory (Thom, 1972)], either two or zero acoustical rays go through a given point, depending on which side (''illuminated'' or ''shadow'' side) of the caustic this point lies on (Fig. 1). For a point on the illuminated side, among the two rays going through this point, one (the so-called *incoming ray*) has not yet tangented the caustic, whereas the other one (the so-called *outgoing ray*) has already tangented the caustic. Sufficiently far from the caustics, these two rays do not interact and sound propagates according to the laws of geometrical acoustics. However, close to the caustics, the two rays become indiscernable [according to the terminology of Kravtsov and Orlov (1993)]. There, diffraction effects must be taken into account to limit the amplitude of the acoustical field. The thickness δ of the diffraction boundary layer (Buchal and Keller, 1960) around the caustic can be chosen as the distance at which the arrival times of the incoming and outgoing signals differ by less than the period of the signal (if periodic), or its duration (for a pulse). Let us choose the origin O at some point of the fold caustic, and introduce the Cartesian coordinate system $(Oxyz)$, with Ox being tangent to the caustic at point O and oriented towards the direction of the ray tangenting the caustic at this point, and Oz being oriented in the normal direction to the caustic, towards the illuminated side. At point O, we denote by ρ_0 the ambient density, c_0 the ambient sound speed, and p_0 the ambient pressure. The radius of curvature of the intersection of the caustics with the (Oxz) plane is $R_{\rm sec}$, while $R_{\rm ray}$ is the radius of curvature of the projection of the acoustical ray on the (Oxz) plane and $R_{\rm cau}=1/(1/R_{\rm sec}+1/R_{\rm ray})$ is the radius of curvature of the acoustical ray relative to the caustics. To formulate the problem in a dimensionless form, three characteristic quantities are introduced:

(1) the characteristic duration of the acoustical signal: $T_{\rm ac}$,
(2) the thickness of the diffraction boundary (Buchal and Keller, 1960): $\delta=(2/c_0^2T_{ac}^2R_{\rm cau})^{-1/3}$, and
(3) the maximal pressure p_{ac} of the incoming acoustical signal at distance δ from the caustic.

According to the catastrophe theory (Berry, 1976), the pressure near the fold caustic can be shown in the high-frequency limit to be a function of two independent variables only: the distance to the caustic z, and the phase of the signal. The corresponding dimensionless variables are

(1) the dimensionless delayed time: $\bar{\tau}=[t-x(1-z/R_{\mathrm{sec}})/c_0]/T_{\mathrm{ac}}$,
(2) the dimensionless distance to the caustic: $\bar{z}=z/\delta$, and
(3) the dimensionless pressure: $\bar{p}=(p-p_0)/p_{\mathrm{ac}}$.

In writing the Euler equations in terms of these variables, the pressure field can be shown to satisfy the nonlinear Tricomi equation (Guiraud, 1965; Hayes, 1968):

$$\frac{\partial^2\bar{p}}{\partial\bar{z}^2}-\bar{z}\frac{\partial^2\bar{p}}{\partial\bar{\tau}^2}+\frac{\mu}{2}\frac{\partial^2(\bar{p}^2)}{\partial\bar{\tau}^2}=0, \tag{1}$$

where coefficient μ measures the nonlinear effects relative to the diffraction effects:

$$\mu=2\beta\mathrm{M}_{\mathrm{ac}}\left[\frac{R_{\mathrm{cau}}}{(2c_0T_{\mathrm{ac}})}\right]^{2/3}, \tag{2}$$

with $\beta=1+B/2A$ the nonlinearity parameter of the medium, and M_{ac} the acoustical Mach number ($\mathrm{M}_{\mathrm{ac}}=P_{\mathrm{ac}}/(\rho_0c_0^2)$).

The associated boundary conditions of the nonlinear Tricomi equation are written below.

(1) In time, for a transient signal, the medium is not perturbed before or after the acoustical wave has passed:

$$\bar{p}(\bar{z},\bar{\tau}\to\pm\infty)=0; \tag{3}$$

or, for a periodic signal (with a period T), one simply gets

$$\bar{p}(\bar{z},\bar{\tau}+T)=p(\bar{z},\bar{\tau}). \tag{4}$$

(2) Away from the caustic in the shadow zone, the acoustical pressure decays exponentially:

$$\bar{p}(\bar{z}\to-\infty,\bar{\tau})\to0. \tag{5}$$

(3) Away from the caustic on the illuminated side, the field matches the geometrical acoustics approximation:

$$\bar{p}(\bar{z}\to+\infty,\bar{\tau})=\bar{z}^{-1/4}[F(\bar{\tau}+\tfrac{2}{3}\bar{z}^{3/2})+G(\bar{\tau}-\tfrac{2}{3}\bar{z}^{3/2})]. \tag{6}$$

The F function is the (dimensionless) time waveform of the *incoming* signal, before it is affected by diffraction while tangenting the caustic. Therefore, the F function is supposed to be known. On the contrary, the G function is the time waveform along the outgoing ray. Unlike the incoming signal F, the outgoing signal G has undergone the diffraction effects after having tangented the caustic, and is unknown. To eliminate this unknown function, the matching boundary condition Eq. (6) can be written as a ''radiation condition,'' by a combination of its derivatives with respect to $\bar{z}$ and $\bar{\tau}$:

$$\bar{z}^{1/4}\frac{\partial\bar{p}}{\partial\bar{\tau}}+\bar{z}^{-1/4}\frac{\partial\bar{p}}{\partial\bar{z}}\xrightarrow[\bar{z}\to+\infty]{}2\frac{dF}{d\bar{\tau}}\left(\bar{\tau}+\frac{2}{3}\bar{z}^{3/2}\right). \tag{7}$$

In Eq. (7), the term $-\frac{1}{4}\bar{z}^{-3/2}[F(\bar{\tau}+\frac{2}{3}\bar{z}^{3/2})+G(\bar{\tau}-\frac{2}{3}\bar{z}^{3/2})]=O(1/z^{3/2})$ coming from the derivative of the slowly varying amplitude is omitted since it is negligibly small compared to other terms $O(1)$ of Eq. (7) emanating from the derivative of the rapidly varying phase.

However, in this new formulation now appears the time derivative of the incoming signal. In the case of an incoming shock wave, this leads to a boundary condition with a sharp singularity (delta Dirac distribution), which is not well suited to a numerical treatment. In order to avoid this difficulty, the problem will now be formulated in terms of potential, instead of pressure.

III. THE NUMERICAL ALGORITHM

A. The equation for the potential

From now on, we drop all subscripts—for the dimensionless variables. The acoustical potential is related to the acoustical pressure by the expression:

$$p=\frac{\partial\phi}{\partial\tau}\Leftrightarrow\phi=\int_{-\infty}^{\tau}p(\tau')d\tau', \tag{8}$$

the (arbitrary) value of the potential at large negative times being chosen equal to 0.

The equation satisfied by the potential field near the caustic now is

$$\frac{\partial^2\phi}{\partial z^2}-z\frac{\partial^2\phi}{\partial\tau^2}+\frac{\mu}{2}\frac{\partial}{\partial\tau}\left[\left(\frac{\partial\phi}{\partial\tau}\right)^2\right]=0. \tag{9}$$

It turns out to be exactly the nonlinear Tricomi Eq. (1), except for the nonlinear term. Equation (9) is called the Tricomi equation for potential.

The associated boundary conditions in time Eqs. (3) and (4) and in the shadow zone Eq. (5) are identical for the potential as for the pressure field. Only the matching boundary condition with geometrical acoustics [Eq. (6) or (7)] is different:

$$z^{1/4}\frac{\partial\phi}{\partial\tau}+z^{-1/4}\frac{\partial\phi}{\partial z}\xrightarrow[\bar{z}\to+\infty]{}2F\left(\tau+\frac{2}{3}z^{3/2}\right). \tag{10}$$

In this ''weak'' formulation, the original incoming signal F now appears instead of its time derivative. Therefore, this formulation is better suited to a numerical resolution in case the incoming signal displays some shocks, as for sonic booms.

B. The iterative scheme

A usual way for solving nonlinear equations involving only boundary conditions (and no initial condition) is to build an iterative scheme, starting from an arbitrary initial condition and converging after several iterations towards the solution of the problem. Following Auger and Coulouvrat (2002), we introduce the so called ''*pseudo time*'' t, through an additional term in the nonlinear Tricomi equation:

$$\frac{\partial^2\phi}{\partial\tau\partial t}=\frac{\partial^2\phi}{\partial z^2}-z\frac{\partial^2\phi}{\partial\tau^2}+\frac{\mu}{2}\frac{\partial}{\partial\tau}\left[\left(\frac{\partial\phi}{\partial\tau}\right)^2\right]. \tag{11}$$

with the unmodified boundary conditions Eqs. (3)–(5) and (10).

The additional term $\partial^2\phi/\partial\tau\partial t$ is supposed to tend toward zero when the iterative solution $\phi(t,\tau,z)$ has reached its ''steady'' limit for large values of the pseudo time t. In this case, $\phi(t\to+\infty,\tau,z)$ satisfies the right-hand side of Eq. (11), i.e., the nonlinear Tricomi equation for potential Eq. (9). The new Eq. (11) is called the ''unsteady'' nonlinear Tricomi equation. It is of hyperbolic type, generally consid-

ered as easier to solve numerically than a mixed (elliptic/hyperbolic) type equation such as the original nonlinear Tricomi equation. The artificial variable t is labeled as a pseudo time for its use to design the iterative process. However, the unsteady nonlinear Tricomi Eq. (11) can be shown to effectively model the diffraction of nonlinear acoustical waves in the shadow zone created by atmospheric refraction (Coulouvrat, 2002). In this case, the (now physical) variable t has the meaning of the penetration distance of the wave inside the shadow zone. Moreover, if the $z\partial^2\phi/\partial\tau^2$ term is omitted in Eq. (11), this one reduces to the well-known KZ equation (Zabolotskaya and Khokhlov, 1969) describing the diffraction of finite amplitude paraxial sound beams. The KZ equation is also a model equation for the diffraction of nonlinear acoustical waves at cusp caustics (Coulouvrat, 2000), the caustics immediately following the fold caustics in the hierarchy of catastrophe theory.

The numerical resolution of the unsteady nonlinear Tricomi Eq. (11) is achieved by means of the fractional steps method (Ames, 1977). Over a single integration step Δt for pseudo time, the equation is split into two simpler equations. The first one takes into account the linear diffraction effects (unsteady linear Tricomi equation):

$$\frac{\partial^2\phi}{\partial\tau\partial t}=\frac{\partial^2\phi}{\partial z^2}-z\frac{\partial^2\phi}{\partial\tau^2}, \tag{12}$$

while the second one takes into account the nonlinear effects (inviscid Burgers' equation for the potential):

$$\frac{\partial\phi}{\partial t}=\frac{\mu}{2}\left(\frac{\partial\phi}{\partial\tau}\right)^2. \tag{13}$$

Starting from the previous iteration i, first Eq. (12) is solved numerically over the pseudo time step Δt, thus providing the intermediate iteration $i+1/2$. This one is used as a starting point for solving Burgers' Eq. (13) over the same pseudo step Δt and finally obtaining iteration $i+1$. This process is repeated until convergence. As a result, both physical mechanisms (linear diffraction and nonlinearities) are taken into account over one pseudo time step. The method of fractional steps is rather common and has been applied successfully for standard algorithms in nonlinear acoustics solving the KZ equation, either in the frequency (Frøysa *et al.*, 1993) or in the time domain (Lee and Hamilton, 1995). Here, it is all the more suited as intermediate steps have no physical meaning, and are just a way to reach convergence toward the solution of the Tricomi's equation. The criterium for convergence simply consists in comparing two successive iterations. If they differ by less than a small parameter ε, then the program is stopped, otherwise the iterative process goes on. Finally, once convergence is reached, the pressure field is derived from the potential by using a standard finite difference scheme (centered derivatives). The choice of the arbitrary parameter ε is discussed in Sec. IV.

C. Resolution of the unsteady linear Tricomi equation

The unsteady linear Tricomi Eq. (12) with boundary conditions Eqs. (3)–(5) and (10) is solved in the frequency domain, using a FFT algorithm. For each frequency, derivatives with respect to $\bar{z}$ are approximated by finite differences precise at second order (centered differences, except for the boundary conditions). Estimation of iteration $i+1/2$ is obtained through a first-order, implicit finite scheme in variable t. Finally, the resulting quasi-tridiagonal linear matrix system is solved using a standard algorithm, and the potential in the time domain is recovered after an inverse Fourier transform. As the procedure is completely identical to the one used by Auger and Coulouvrat (2002), further details are not repeated here. The only difference is that, in the boundary condition Eq. (10), there now appears the incoming time waveform $F(\tau)$ instead of its time derivative in the algorithm of Auger (2001). For incoming shock waves (such as an N wave for sonic boom), the time waveform is much less singular than its derivative. Indeed, as the potential is a continuous function, solving the problem in terms of potential instead of pressure leads to a suppression of Gibbs oscillations that resulted from the Fourier transform of the discontinuous pressure field. While these oscillations could be sharply reduced through the iterative process of Auger and Coulouvrat (2002) by adding some small numerical viscosity in the discretization of Burgers' equation, this reduction was achieved only after a sufficient number of iterations, and convergence required several thousands of iterations. Now, with the new algorithm for the potential, convergence is reached after a few tens of iterations only.

The choice of an algorithm in the frequency domain is motivated by the transsonic aspect of the Tricomi equation. Let us recall that a Tricomi equation is of mixed type, either hyperbolic if $z-\mu p>0$, or elliptic otherwise, the sonic line $z-\mu p=0$ separating the illuminated (or supersonic) side of the caustics where sound "propagates," from the shadow (or subsonic) side where sound is evanescent. In the elliptic domain below the sonic line, there is no oriented flow of information in time τ, contrarily to the hyperbolic domain where information propagates along the sense of ascending times. This difference of behavior was the key point of the original algorithm of Murman and Cole (1971) for transsonic problems, which introduced a switch in the way of discretizing the transsonic equations, using upwind finite differences in the hyperbolic domain but centered finite differences in the elliptic domain. Such a way of discretizing is therefore incompatible with a time domain algorithm for the KZ equation such as the one used by Lee and Hamilton (1995), which relies heavily on the hyperbolic character of the KZ equation and the oriented flow of information along ascending times. The use of an algorithm in the frequency domain implies an artificial periodicity of the problem (the period being the size of the computation domain in time). Imposing this periodicity, it forces some reverse flow of information, hence removing the problem of specifically handling the flow of information in the elliptic domain. This can be seen as an equivalent to the hyperbolic wave equation (with its associated initial conditions in time) being transformed in the frequency domain into the elliptic Helmholtz equation (with no initial conditions). The numerical cost to pay for this is that the method requires a sufficiently large domain in time compared to the effective duration of the signal, so that the artificial periodization of the signals interferes as little as pos-

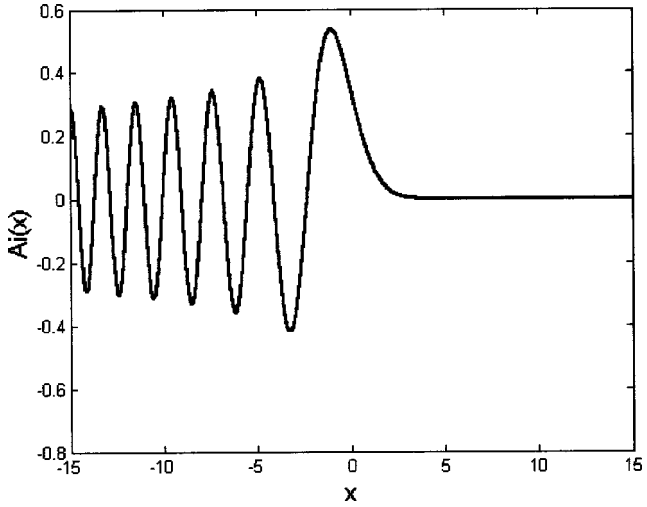

FIG. 2. The Airy function.

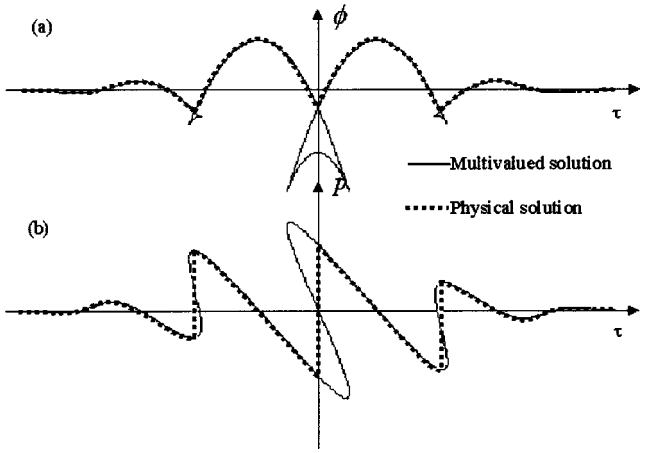

FIG. 3. Multivalued and physical solutions of the inviscid Burgers' equation (a) for potential and (b) for pressure.

sible with the signal. This appears perfectly manageable from a computational point of view by choosing for an incoming "N" wave of duration 1 a time domain equal to $[-8/3;+11/3]$. A second justification for the choice of an algorithm in the frequency domain is that, in the linear case $\mu=0$, the exact solution of the Tricomi equation can be obtained as a superposition of Airy functions (Gill and Seebass, 1973). In catastrophe theory, the Airy function (1838) is the generic solution for the pressure field near fold caustics (Berry, 1976) and reflects the mixed elliptic/hyperbolic type of the Tricomi equation through its oscillating or exponentially decaying character, depending on the sign of its argument (Fig. 2). Moreover, for sonic boom, the nonlinear parameter μ in Tricomi equation is generally small, of the order of 0.1. This means that the main effect of nonlinearities is to limit the amplitude of the "U" wave (unbounded in the linear case), according to the scheme intuited by Guiraud (1965). Therefore the solution of the nonlinear Tricomi equation deviates only weakly from the linear solution, which is "naturally" given in the frequency domain by the Airy function.

D. Analytical solution of the inviscid Burgers equation

In the algorithm of Auger and Coulouvrat (2002), the inviscid Burgers' equation for the pressure field was solved numerically using a *shock capturing* algorithm of McDonald and Ambrosiano (1984). The chosen scheme discretizes the Burgers' equation by using either first-or second-order finite differences. Generally, more precise second-order differences are used, however, near shock waves, first-order differences are preferable as they introduce numerical viscosity that stabilizes the algorithm and enable to go through (to capture) the shock. The "switch" between first- and second-order differences is made through a filter that guarantees monotonicity. As an explicit scheme, it imposes a CFL stability condition that prevents the use of relatively large Δt steps. In the present version of the algorithm, the *shock* capturing scheme has been replaced by an "exact" *shock fitting* algorithm. It is based on the graphical method used by Hayes *et al.* (1969) in the so-called ARAP sonic boom propagation code for solving Burgers' equation along the acoustical rays launched by the aircraft. The algorithm is based on the exact solution of the Burgers' Eq. (13) expressed for the pressure field:

$$\frac{\partial p}{\partial t}=\frac{\mu}{2}\frac{\partial (p)^2}{\partial \tau}. \tag{14}$$

Note that variable t (pseudo time) plays the role of a distance of propagation in the usual formulation of the inviscid Burgers' equation in nonlinear acoustics. For an initial condition $p(t=0,\tau)=p_0(\tau)$, the solution of Eq. (14) is given under the implicit form by the Poisson's solution (Blackstock *et al.*, 1998):

$$\begin{aligned} &p(t,\tau)=p_0(\theta)\\ &\tau=\theta-\mu t p_0(\theta), \end{aligned} \tag{15}$$

where θ is the nonlinear characteristic variable associated to the distorsion of the wave profile. If the distance of propagation t is higher than the shock formation distance t_c, then this solution is multivalued, and hence physically meaningless. Shocks must be introduced, their position being determined according to the weak shock theory [such as in Pestorius algorithm (1973)], or equivalently by applying the law of equal areas (Landau, 1945). However, these methods are rather complex to implement numerically, especially for dealing with the emergence of new shocks, or the merging of several shocks into a single one, phenomena that are likely to occur for the Tricomi equation, especially near the sonic line where the shock pattern may be rather complex. The method of Hayes based on the potential turns out much simpler to code. First, Poisson's solution for the potential Eq. (13) with the initial condition $\phi(t=0,\tau)=\phi_0=\int_{-\infty}^{\tau}p_0(\tau')d\tau'$ is [θ being implicitly defined by relation (15)]

$$\phi(t,\tau)=\phi_0(\theta)-\frac{\mu t}{2}(p_0(\theta))^2. \tag{16}$$

As for the pressure, if the propagation "distance" is larger than the shock formation distance $t>t_c$, this solution is multivalued. However, Hayes *et al.* (1969) noted that, among the multiple possible values of the potential, the physically

meaningful one is the maximum of potential [Fig. 3(a)]. This result is directly related to the second principle of thermodynamics and the fact that shock waves of Burgers' equation can only be compression shock waves. The positions of shock waves are therefore automatically determined as the intersections of the several branches of the multivalued Poisson's solution. In short, the exact solution, including shock waves, is simply

$$\phi(t,\tau)=\max\left\{\phi_0(\theta)-\frac{\mu t}{2}(p_0(\theta))^2\right\}. \tag{17}$$

From a numerical point of view, finding the maximum of several values is much more efficient than solving the differential equation governing the position of the shocks according to weak shock theory, or determining the position that makes the surface of the two lobes equal, as for the law of equal areas. The only numerical cost is due to the discretization. Indeed, the initial condition is given numerically on an equally spaced grid. This means that the exact Poisson's solution is known for equally spaced discrete values of the characteristic variable θ. As a counterpart, the discrete values of the physical variable τ are unequally spaced. To compare the different values of the multivalued solution Eq. (16) for the *same* value of τ, it is therefore necessary to reinterpolate the multivalued solution on a *fixed*, equally spaced grid for the τ variable. This is the only numerical approximation that is introduced into the scheme, otherwise the method is analytically exact. In particular, it can be applied for whatever value of the pseudo time step Δt. There is no CFL condition.

Note that this method allows us to find the physical pressure too, since the physical points for the Poisson's solution in pressure are the points corresponding to the physical potentiel [Fig. 3(b)]. More details on the overall algorithm illustrated by a diagram can be found in Auger and Coulouvrat (2002). In the present up-dated version, the only changes in that diagram consist in replacing the pressure by the potential, and the MacDonald and Ambrosiano algorithm by the analytical solution Eq. (17).

IV. VALIDATION OF THE ALGORITHM

A. Convergence down to machine precision

Convergence tests have shown that the convergence parameter ε can be chosen arbitrarily small, down to machine precision ($\varepsilon \approx 10^{-15}$) (Fig. 4). This is a crucial test to check the effective convergence of the whole numerical process (iterative unsteady Tricomi equation+split step +discretisation) towards the solution of the nonlinear Tricomi equation. However, in practice, such an extreme precision is not necessary, and we routinely choose $\varepsilon \approx 10^{-7}$. Using this parameter the computation time is dramatically reduced with a factor of 40 in comparison with the existing code of Auger and Coulouvrat (2002). This factor grows exponentially with the criterion of convergence. This is an important difference between the two methods, that proves the potential formulation associated with an explicit treatment of nonlinearity is more pertinent than the associated pressure formulation.

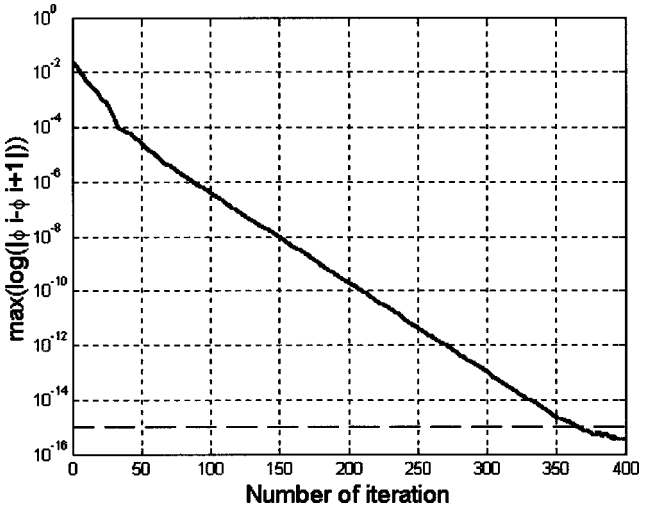

FIG. 4. Logarithm of the maximal value of the difference between two successive iterations i and $i+1$ versus the number of iterations, for an incoming N wave with $\mu=0.05$.

B. Convergence with mesh grid refinement

When nonlinearities are neglected ($\mu=0$), the solution of the linear Tricomi's equation for pressure for an incoming shock wave is singular (logarithmic singularity on the illuminated side, power $-\frac{1}{6}$ on the geometrical caustic). This singularity is impossible to reproduce numerically because of the filtering induced by discretization, but we observe a regular increase of the maximal pressure amplitude with the number of discretization points. As the exact mathematical solution is singular, the numerical one does not converge with grid refinement (Fig. 5). This behavior is of course physically meaningless and, according to Guiraud (1965), nonlinearities must be introduced to remove the singularity when the incoming wave has a shock. This expected behavior is observed numerically in Fig. 5, where we clearly get numerical convergence for a sufficiently fine grid (1024 discretization points in time or more). Also, the nonlinear solution strongly deviates from the linear one. This result is an indirect validation of the algorithm, showing that it follows Guiraud's assumption, and better converges with time discretization than the previous algorithm of Auger and Coulouvrat (2002). Let us finally notice that, contrarily to the time discretization, the number of points in distance z does not influence very much the solution.

C. Physical behavior

For incoming ''N'' waves, the numerical solution depends only on the physical nonlinearity parameter μ. Figures 6 and 8 show the spatio-temporal field of pressure $p(z,\tau)$ in a linear grayscale calculated along a line perpendicular to the caustic versus dimensionless time for $\mu=0.05$ and $\mu=0.5$. The white line is the sonic line separating the elliptic (shadow) zone from the hyperbolic (illuminated) one. The deformation of the sonic line is very sensitive to the nonlinearity parameter. In the hyperbolic zone, cusped wavefronts are obvious, corresponding to each incoming and outgoing shock waves. For both values of μ, the incoming and outgo-

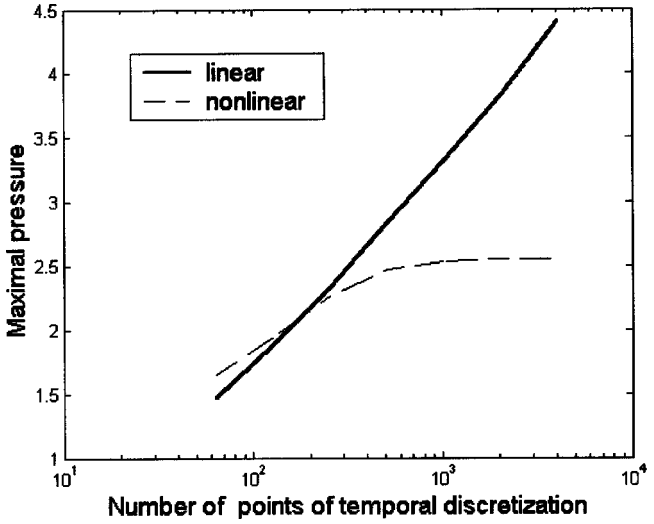

FIG. 5. Maximal value of the dimensionless pressure versus the number of points of the temporal discretization (1500 points in the spatial grid) in the linear case ($\mu=0$) and in the nonlinear case ($\mu=0.1$), for an incoming N wave.

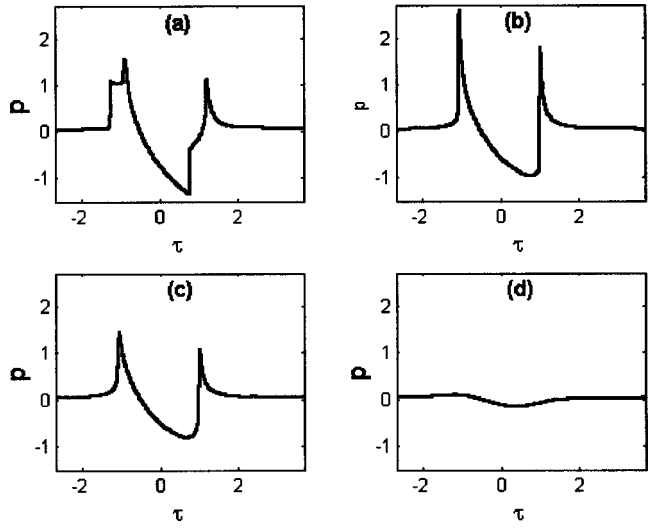

FIG. 7. Pressure versus dimensionless time for $\mu=0.05$, for four distances from the caustic: (a) $z=1$, (b) $z=z_{\max}$ (distance where the maximal pressure is found), (c) $z=0$, and (d) $z=-1$.

ing shocks merge exactly on the sonic line. No triple shock is observed. In the shadow zone, no shock propagates in accordance with the elliptic nature of the equation there. For both values of μ, the signal is also plotted at several distances from the caustic (Figs. 7 and 9). At matching distance with geometrical acoustics $z=1$ [Figs. 7(a) and 9(a)] the incoming and the outgoing signals are similar to test flights measurements (Wanner *et al.*, 1972): the ''N'' wave is transformed into a ''U'' wave. The higher the nonlinearity parameter, the more the solution is distorted is. Figures 7(b) and 9(b) show the pressure versus time at the distance where pressure is maximal. The amplification factor (maximal amplitude divided by the amplitude of the ''N'' wave at the matching boundary) decreases as the nonlinearity parameter increases: it is about 2.5 for $\mu=0.05$, but only 1.5 for $\mu=0.5$. For the value $\mu=0.05$ typical for sonic boom, the amplification factor is in agreement with flight tests values. On the geometrical caustic [$z=0$, Figs. 7(c) and 9(c)], the amplitude has strongly decreased because the first peak is now in the shadow zone. This is completely different from the linear behavior, where the highest singularity is right on the geometrical caustic. In the nonlinear case, the point of maximum amplitude is generally in the elliptic domain, very close to, but not exactly on, the sonic line. Note that for strong nonlinearities [Fig. 9(c)], the signal deviates from the usual ''U'' shape, as the first peak is strongly smoothed because in the shadow zone, while the second one remains sharp because still in the hyperbolic domain. Finally, away in the elliptic zone [Figs. 7(d) and 9(d), $z=-1$], the signal is smooth, and its amplitude is very weak as expected, due to the exponential decay there. These results, showing the numerical simulations behave qualitatively as expected from the physics and in agreement with flight tests, provide an additional validation.

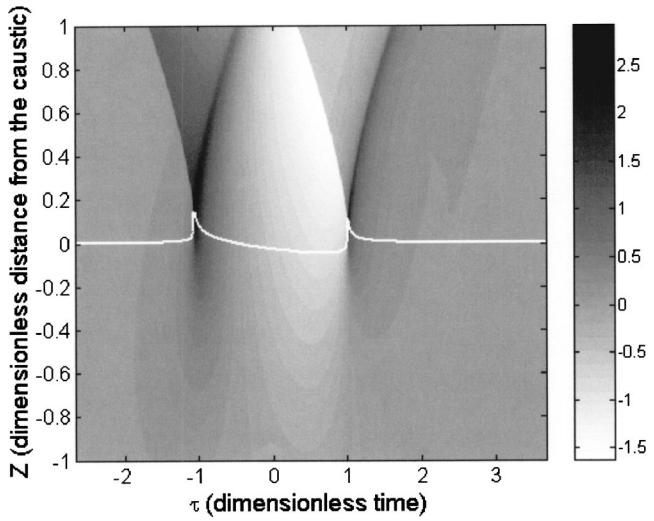

FIG. 6. Pressure field for $\mu=0.05$. The white line is the sonic line. The hyperbolic zone is above that line, the elliptic one is below. The pressure levels are indicated by the gray bar.

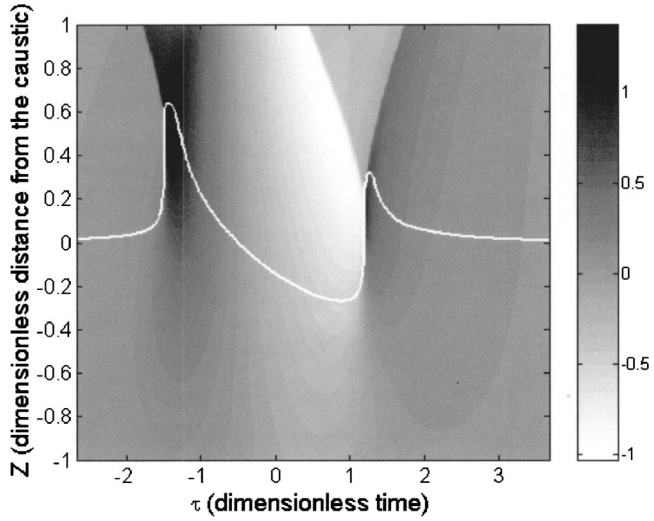

FIG. 8. Pressure field for $\mu=0.5$. The white line is the sonic line. The hyperbolic zone is above that line, the elliptic one is below. The pressure levels are indicated by the gray bar.

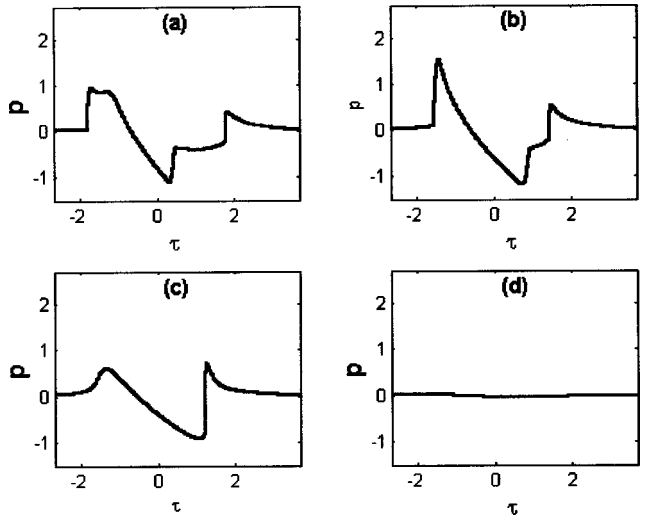

FIG. 9. Pressure versus dimensionless time for $\mu=0.5$, for four distances from the caustic: (a) $z=1$, (b) $z=z_{\max}$ (distance where the maximal pressure is found), (c) $z=0$, and (d) $z=-1$.

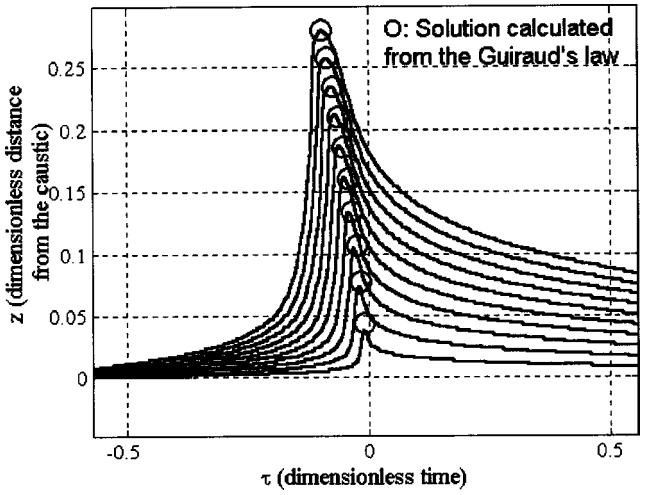

FIG. 10. Validation of Guiraud's similitude for an incoming rectangular window signal. Computed deformation of the sonic line for different values of μ between 0.01 and 0.2 (continuous lines) and comparison with Guiraud's similitude for the point of maximum deformation (circles).

D. Guiraud's similitude

It has been established previously that the numerical solution converges toward a finite value. To ensure this value is correct, and to provide a quantitative validation of the code, we check the similitude law derived by Guiraud (1965). Indeed, with the new scaling: $\phi=\mu\tilde{\phi}$, $z=\mu^{4/5}\tilde{z}$, and $\tau=\mu^{6/5}\tilde{\tau}$, the nonlinear Tricomi equation can be written

$$\frac{\partial^2\tilde{\phi}}{\partial\tilde{z}^2}-\tilde{z}\frac{\partial^2\tilde{\phi}}{\partial\tilde{\tau}^2}+\frac{1}{2}\frac{\partial}{\partial\tilde{\tau}}\left[\frac{\partial\tilde{\phi}}{\partial\tau}\right]^2=0, \tag{18}$$

and its boundary condition

$$\tilde{z}^{1/4}\frac{\partial\tilde{\phi}}{\partial\tilde{\tau}}+\tilde{z}^{-1/4}\frac{\partial\tilde{\phi}}{\partial\tilde{z}}=2F\left(\mu^{6/5}\left[\tilde{\tau}+\frac{2}{3}\tilde{z}^{3/2}\right]\right). \tag{19}$$

Note that the nonlinearity parameter is eliminated from the nonlinear Tricomi equation, but now appears in the phase of the boundary condition. However, for a ''step'' wave [$F(\tau)=0$ for $\tau<0$ and $F(\tau)=1$ for $\tau>0$], the incoming wave profile is invariant by a phase dilatation, so the whole problem gets independant of the value of μ. The objective of the validation test is to check whether the code satisfies this property. However, because of the discretization, a true step shock of infinite duration cannot be simulated. Instead, we use a rectangular window [$F(\tau)=1$ if $0<\tau<2$ and $F(\tau)=0$ everywhere else]. This function is completely identical to the step function locally around the shock, so that we can expect it to satisfy at least approximately Guiraud's scaling law. This kind of approximation is used in practice by Gill and Seebass (1973) to estimate solutions of the nonlinear Tricomi equation when the hodograph transform fails to predict the shock positions. For the pressure field, the correct similitude is $p=\mu^{-1/5}\tilde{p}$. Guiraud's similitude is tested in Fig. 10 for the amplitude and position of the maximal distorsion of the sonic line, corresponding to the cusp of the shock wavefront on the sonic line. This point is chosen as it is exactly on the shock wavefront, so that it is as little as possible influenced by the finite duration of the signal. Moreover, this point is easily spotted, and especially difficult to capture numerically, as convergence there requires a finer discretization than for other points. Therefore, it is a demanding, quantitative test. At this point, according to the scaling law,

$$p_{\max}=\mu^{-1/5}C_p, \tag{20}$$

$$z(p_{\max})=\mu^{4/5}C_z, \tag{21}$$

$$\tau(p_{\max})=\mu^{6/5}C_\tau, \tag{22}$$

where the quantities C_p, C_z, C_τ should be constant if the problem is invariant. Results are plotted in Fig. 10, where the *computed* sonic lines at different values of μ between 0.01 and 0.2 are plotted as continuous lines, while the positions of the cusp (circle) for the same values of μ are *deduced* numerically by Guiraud's scaling law Eqs. (21) and (22) from the computed position at the lowest value of μ. Figure 10 obviously demonstrates this point (circle) constantly remains on the top of the (continuous) sonic line, accordingly to the theoretical similitude. The results are also in very good agreement for the pressure amplitude, as exemplified by Fig. 11: for μ values larger than 0.02, the ratio $\mu^{1/5}p_{\max}$ deviates from less than 2% of the constant value 1.76. The larger deviation for smaller values of μ is related to unsufficient time discretization in cases where the very sharp peaks of the wave profile are difficult to capture numerically. Hence, the numerical scheme satisfies the nonlinear quantitative similitude law. The whole sonic line, and not only the positions of the wavefront cusp, could be theoretically deduced from one another through Guiraud's law. However, if applied for the *finite* signal used here, the similitude would rapidly diverge from numerical simulations. For instance, according to Guiraud's law, the ''width'' of the sonic line around his maximum deformation should be 36 times larger for the largest value of μ than for the smallest one. Clearly this is not the case, because the numerical results are constrained by the *finite* duration of the signal, which prevents too huge distorsions, especially for the phase variable. This explains why,

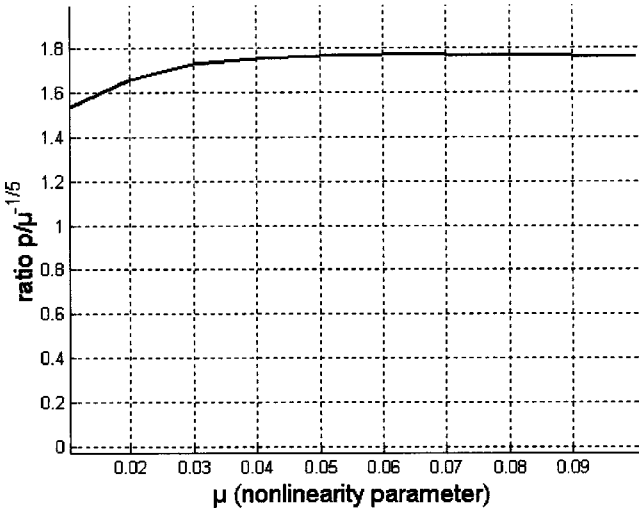

FIG. 11. Validation of Guiraud's similitude: ratio $p_{\max}/\mu^{-1/5}$ as a function of μ for an incoming rectangular window signal and for the wavefront cusp.

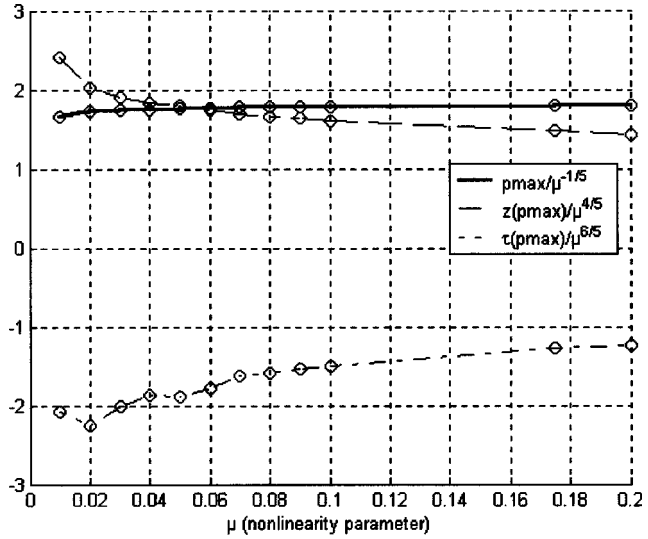

FIG. 12. Validation of Guiraud's similitude: ratios $p_{\max}/\mu^{-1/5}$, $z(p_{\max})/\mu^{4/5}$, and $\tau(p_{\max})/\mu^{6/5}$ as a function of μ for an incoming rectangular window signal and for the point of maximum amplitude.

when applied for the point of maximum amplitude which is slightly *away* from the wavefront cusp inside the elliptic domain, the similitude law remains well satisfied for the pressure amplitude, but not so well for its position (Fig. 12). Indeed, it still satisfies a similitude law, but with a power 0.63 instead of 0.8 for the distance z, and a power 0.99 instead of 1.2 for the phase τ. Similar results can be obtained when the incoming signal is an ''N'' wave. Consequently, when applying Guiraud's similitude, Gill and Seebass (1973) and Plotkin (2002) predict with a rather good accuracy the focused boom peak amplitude, but not so well the precise shape of the superboom.

V. SONIC BOOM SIMULATION OF AN ACCELERATING SUPERSONIC TRANSPORTER

A numerical simulation of focused sonic boom at the ground level has been realized in a ''realistic'' case. The chosen mock-up is the so-called Eurosup configuration (Evans and Doherty, 1997) (Fig. 13), derived from the European ESCT configuration for a future supersonic transport aircraft. It is a wing–body configuration without horizontal canard or aft-tail and without vertical fin. The double delta wing is set in a low position relative to the fuselage which has a circular section and is 89 m long. The wing twist, camber, and thickness have been numerically optimized, and a model has been built for wind-tunnel tests at supersonic and transonic speeds.

Sonic boom focusing has been numerically simulated under the assumption of a horizontal flight at altitude 35 000 ft (10 668 m), with a constant acceleration of 1 m/s^2, and in the standard atmosphere. The altitude is typical for Concorde during its transonic acceleration phase along the route Paris to New York. The acceleration is relatively large, but leads to a ground track focusing at the ground level occurring almost exactly at Mach 1.2. (1.207). Due to atmospheric conditions, the aircraft Mach number for ground track focusing is variable, and Mach 1.2 is considered as a representative ''mean'' value. Anyway, previous simulations have shown (Auger and Coulouvrat, 2002) that the acceleration has little influence on the amplitude of focused sonic boom (but it has on the caustics position). For focusing, only boom simulations in the plane of symmetry (boom emitted with a zero azimutal angle) have been realized.

The computations have been performed by coupling the numerical solver of the Tricomi equation to the numerical code **BANGV** currently being developed by Airbus France SAS and Université Pierre et Marie Curie. It is based on a standard ray model, modified to take into account the non-

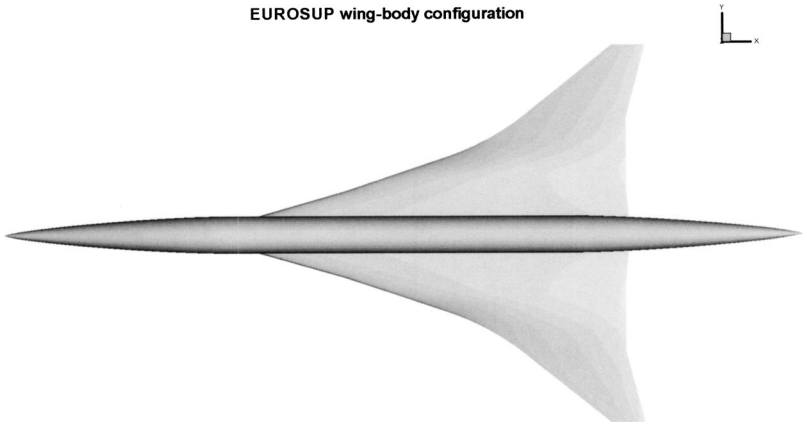

FIG. 13. The Eurosup mock-up.

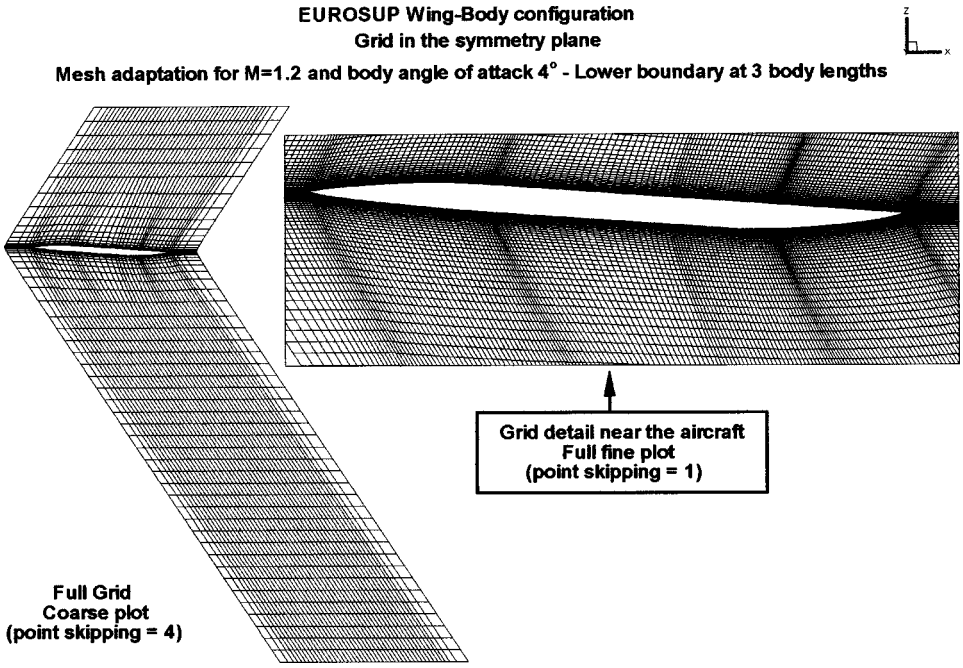

FIG. 14. Mesh grid in the mock-up symmetry plane.

linear distortion of the sonic boom waveform as it propagates from the aircraft down to the ground. Boom is computed along the ray that is tangent to the caustic at the ground until this ray reaches a point slightly above the ground. This provides the incoming waveform $F(\tau)$ and the nonlinear parameter μ that are the only input parameter for the algorithm solving the nonlinear Tricomi equation.

The source term, used as an input pressure field for the sonic boom code, has been determined using CFD simulations of the Euler equations around the mock-up. The finite volume software **elsA** (Cambier, 1999) has been used, with uncentered upwind fluxes of the Roe type. The meshing of the air volume around the mock-up was determined using an analytical method to build a structured grid with an H-type topology. The mock-up is first set at the desired angle of attack before meshing the volume around the configuration so that constant K index surfaces remain always planes parallel to the incoming flow velocity at some distance: this is intended to avoid interpolation errors when extracting the pressure fields in the planes required for the sonic boom code input. The H-type topology of the meshing is especially suited for capturing fine transverse gradients of the pressure field. The meshing was preadapted to the Mach number, by limiting the grid between the two Mach cones emanating from the fuselage at its nose and at its tail (slightly extended forward/backward to be sure to capture all the shock waves emanating from the mock-up, Fig. 14). The computational domain was extended below to 3 fuselage lengths, but to only 1 fuselage length above. For a better capture of the origin of the shock waves, grid refinement was introduced around the Mach cones emanating from the nose, the wing leading edge, the wing trailing edge and the fuselage tail. Far from the mock-up, the grid refinement has to become more regular because the exact position of the shock waves cannot be guessed in advance. This results in the type of meshing shown on Fig. 14 in the plane of symmetry. The 3D meshing was of the order of 5 million computation points.

The matching between the near-field Euler simulations and the acoustical propagation model was not sophisticated, using directly the CFD pressure waveform extracted at some distance from the aircraft as an input for the ray propagation. No ''smooth'' matching as those described by Plotkin and Page (2002) was performed.

Pressure waveforms below the mock-up in the symmetry plane are shown in Fig. 15 for five different distances H (0.5, 1, 1.5, 2, 2.5 fuselage lengths L). For comparison, the pressure fields are normalized by the ratio $\sqrt{H/L}$ to compensate for the geometrical attenuation due to the conical form of the wavefront. If the pressure field would perfectly match the classic Whitham's assumptions for sonic boom theory (slender body, far-field approximation, linear and locally axisymmetric field), these different curves should perfectly superimpose. On the figure we can clearly see three shock waves emanating from the aircraft nose, wing leading edge, and fuselage tail. At $H=0.5L$, we observe a fourth, sharp shock wave emanating from the wing trailing edge, but this one rapidly decays at larger distances. Therefore, it appears as a near-field, local effect, and the distance $H=0.5L$ seems too short for a sound matching with acoustical propagation. The end of the pressure waveform at $H=2.5L$ strongly deviates from the undisturbed value 0, probably due to a mesh boundary too close to the fuselage tail. More generally, the pressure field at the rear appears pretty complex, as confirmed by off-symmetry simulations, and the extent of the meshing is probably too close to the fuselage for capturing precisely the decaying tail of the pressure waveform. On the contrary, the two first shocks seem to superimpose almost perfectly. Small deviations (advancement of the nose shock and attenuation of the small dip ahead of the leading edge shock) can be explained by nonlinear propagation effects that are anyway taken into account in the propagation code. Especially, we do not see any strong deviation from the assumption of locally axisymmetric field, even for the leading edge shock though

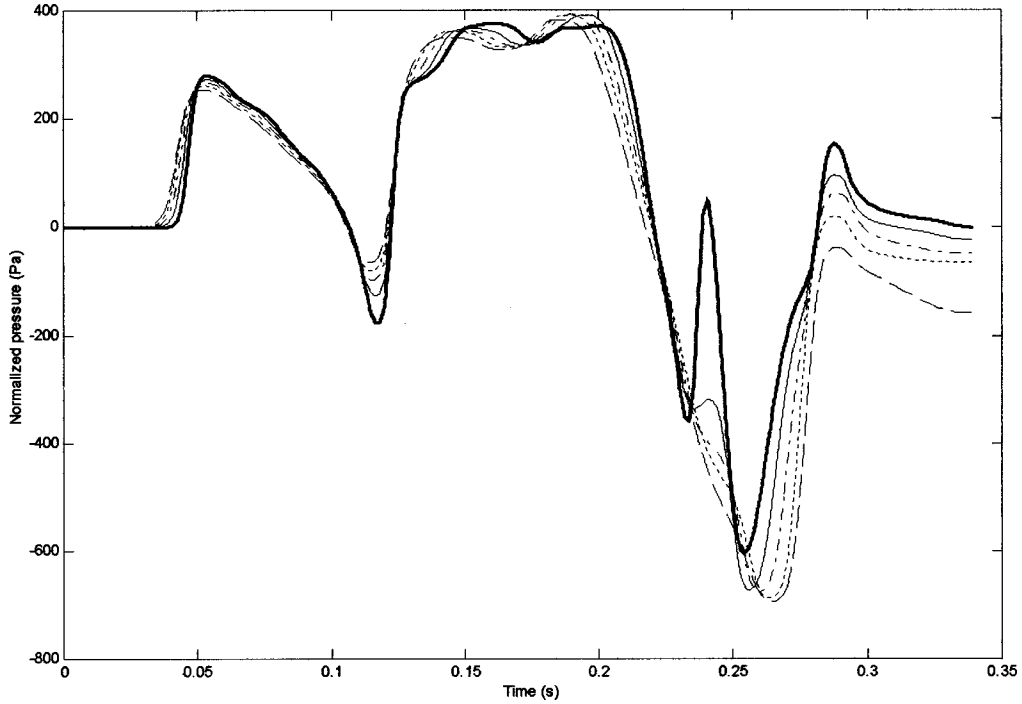

FIG. 15. Normalized pressure waveforms at five different distances below the mock-up (thick line: H/L=0.5, continuous line: H/L=1, dash dotted line: H/L=1.5, dotted line: H/L=2, and dashed line: H/L=2.5).

this one is mostly associated to lift effects that are far from axisymmetric. This point is also confirmed by off-symmetry pressure fields.

Figure 16 shows the ground sonic boom predicted in cruise condition at Mach 1.2 (no acceleration, therefore no focusing), depending on the ratio H/L at which the matching between CFD and the propagation code is realized. For the two head shocks (nose and leading edge), the agreement is almost perfect, which demonstrates the soundness of the whole numerical procedure. The results are not so good for the rear shock, especially for $H/L=0.5$ and 2.5, obviously a consequence of the nearfield simulations (local fourth shock wave at $H/L=0.5$, too short mesh at $H/L=2.5$). The agreement is acceptable for the three other intermediate values, despite some uncertainty in the rear shock position and amplitude. Also noteworthy is the triple shocks structure of the

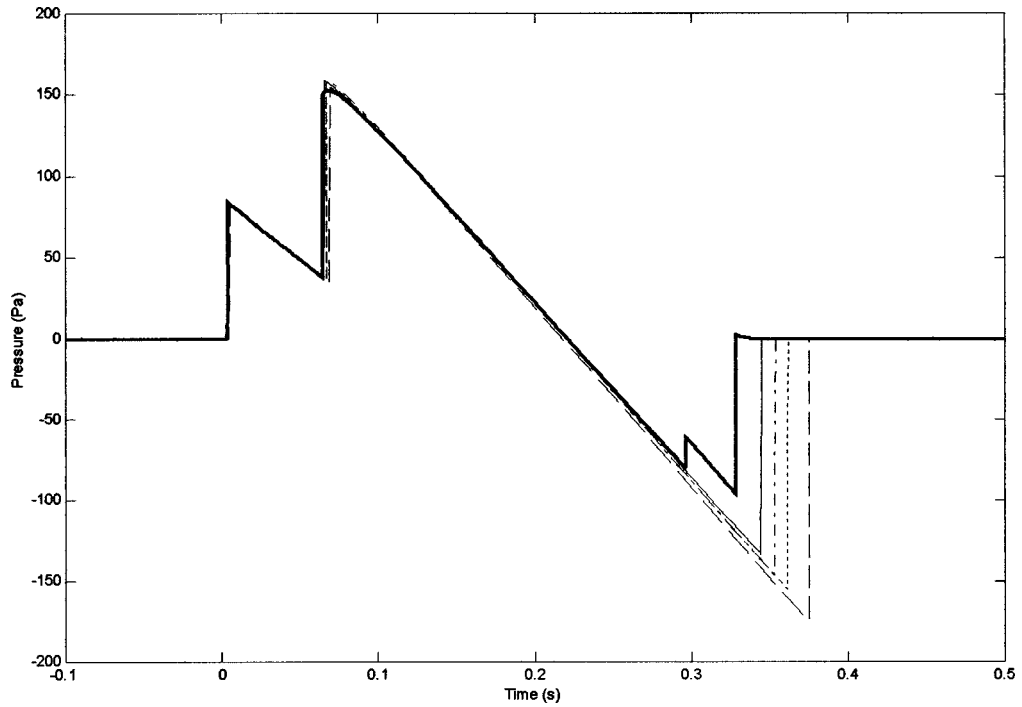

FIG. 16. Ground track sonic boom at cruise Mach number 1.2 computed by matching with CFD Euler simulations at five different distances below the aircraft (thick line: H/L=0.5, continuous line: H/L=1, dash dotted line: H/L=1.5, dotted line: H/L=2, and dashed line: H/L=2.5).

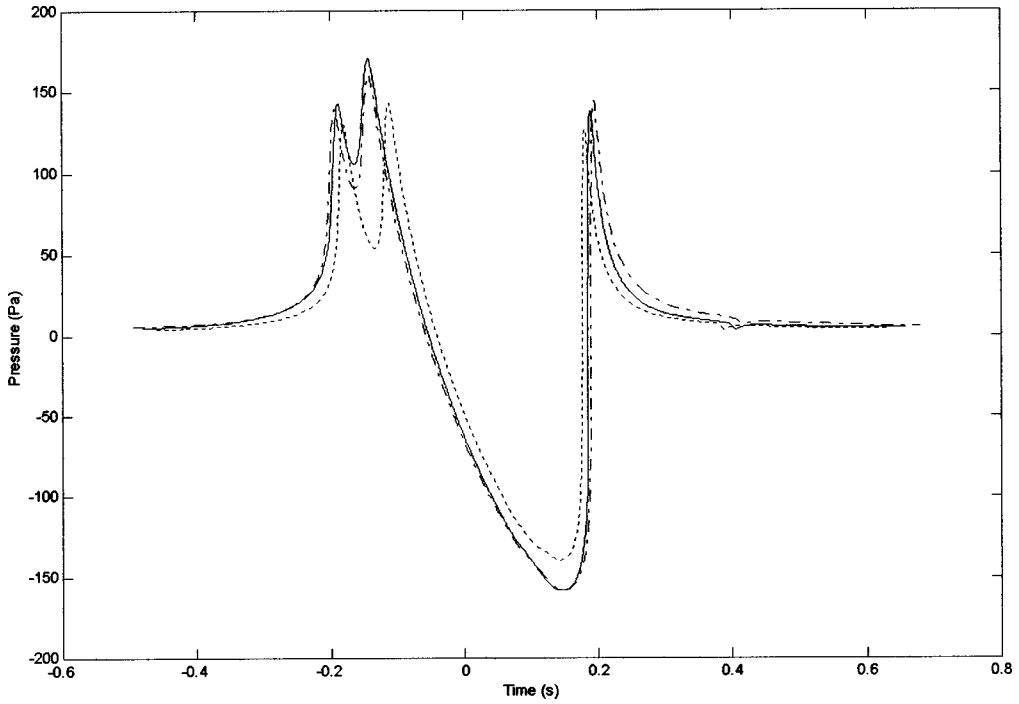

FIG. 17. Groundtrack focused pressure waveforms at the geometrical caustic ($z=0$) for three different matching distances (continuous line: H/L=1, dash dotted line: H/L=1.5, and dotted line: H/L=2).

boom waveform. This is due to the low Mach 1.2 inducing a nose shock rather strong compared to the leading edge shock (roughly 75%, Fig. 15). At Mach 1.2, fly altitude is lower than for a Mach 2 cruise, boom propagation is shorter, and nonlinear effects are not sufficient for the shocks to merge into the classic ''N'' wave boom (which would be observed at Mach 2). For computation of boom focusing, the Tricomi solver perfectly handles such ''complex'' incoming waveforms, contrarily to the aproximate method of Gill and Seebass (1973) valid for noninteracting shock waves, an assumption not satisfied here for the two close head shocks.

Figure 17 shows the computed focused boom right at the geometrical caustics ($z=0$ in the Tricomi equation), only for the three ''admissible'' distances $H/L=1$, 1.5 or 2. Due to the three-shock structure of the incoming waveform, the focused boom exhibits a more complex shape than the usual

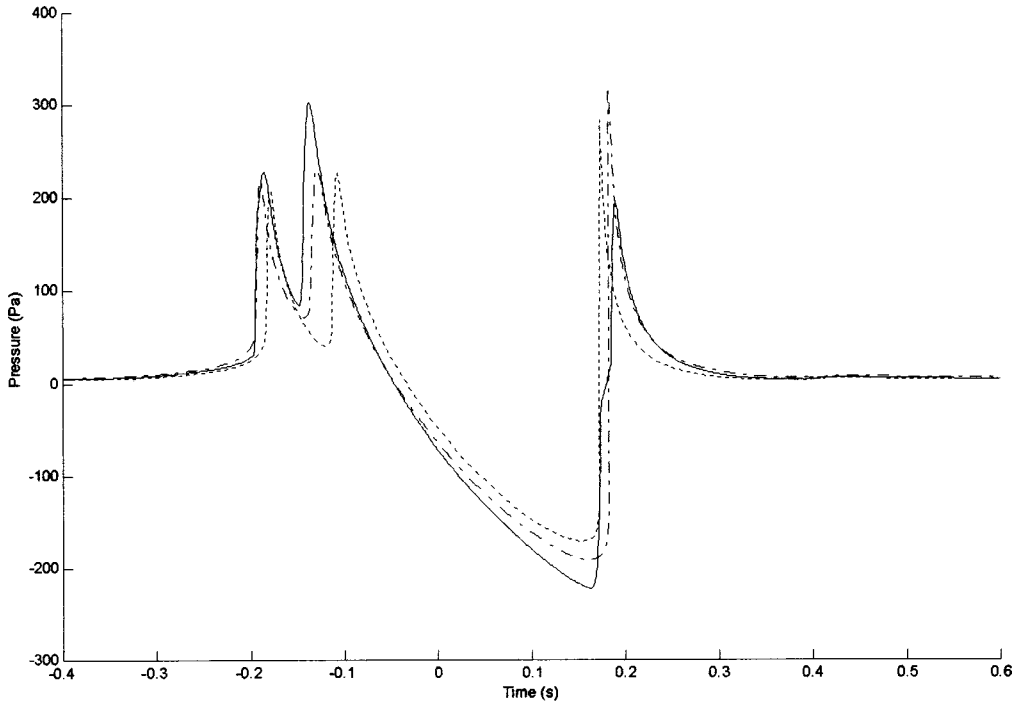

FIG. 18. Groundtrack focused pressure waveforms at the position of maximum amplitude for three different matching distances (continuous line: H/L=1, dash dotted line: H/L=1.5, and dotted line: H/L=2).

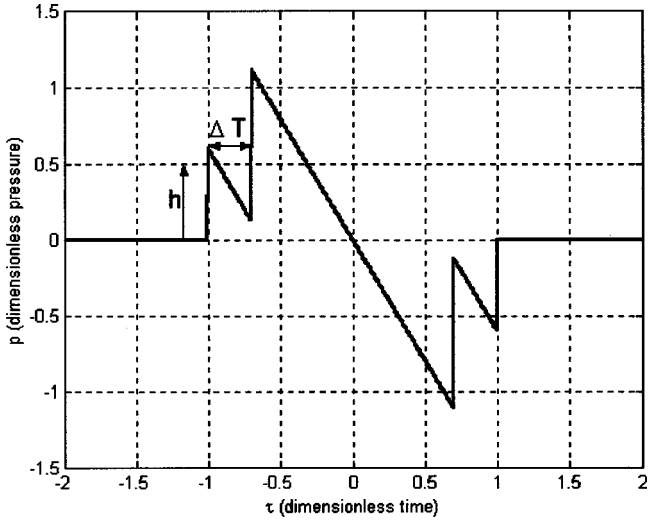

FIG. 19. ''Optimized'' signal where the nose and leading edge shocks have not merged yet.

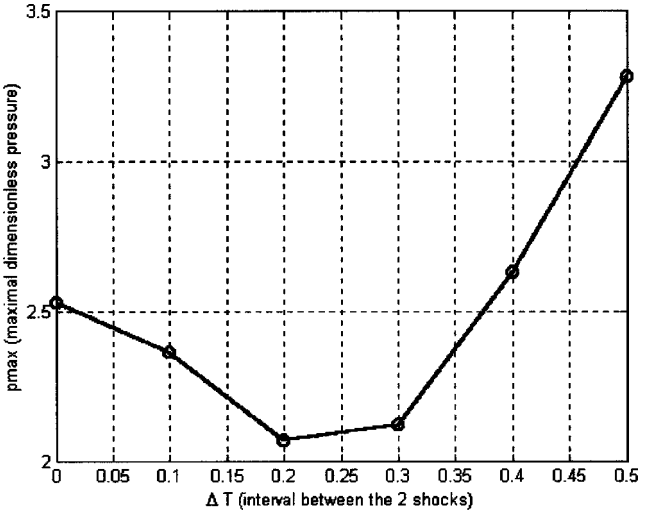

FIG. 20. Maximal overpressure as a function of the time interval between the nose and the leading edge shocks.

''U'' wave, each incoming shock wave giving rise to a peak. The agreement between the three curves turns out to be very satisfying, especially for the first and third ''peaks.'' There is some deviation, however, for the phase of the second shock in the case $H/L=2$, but it has only a marginal consequence on the peak amplitude.

Figure 18 displays the same curves, but now at the distance $z_{\max}$ from the geometrical caustics where the pressure field reaches its peak value. As $z_{\max}$ depends on the input parameter, the three curves of Fig. 18 are not calculated exactly at the same distance $z_{\max}$, a fact that amplifies the differences between the curves compared to Fig. 17. This is especially obvious, for the case $H/L=1$, where the highest peak is associated to the second incoming shock (leading edge), while for the two other cases, it is associated to the third (tail) shock. Let us recall that for an N wave, it is always associated to the first shock! Comparing the two cases $H/L=1.5$ or 2, however, the agreement is very good, the only main difference being once again the phase of the second shock for $H/L=2$. Also to be noticed is the peak amplitude ($\sim$300 Pa for all three cases), significantly different from the one at the geometrical caustics ($\sim$150 Pa). The position $z_{\max}$ is typically of the order of 0.25 times the boundary layer thickness, which corresponds roughly to about 100–200 m. Taking into account the inclination of the caustic relative to the ground plane, this means that the point of maximum pressure may deviate from several hundred meters from the geometrical caustics, a fact that is likely to make test flights measurements of focused boom especially difficult to carry out. Precise numerical simulations such as the present one are all the more attractive.

VI. CONCLUSION: TOWARDS A MITIGATION OF SUPERBOOM?

Finally, a numerical study on the reduction of the focused sonic boom is presented. The solution of the nonlinear Tricomi equation is presented for several incoming waveforms. We choose to compare a signal where the shocks due to the nose and the leading edge have not merged yet, as for the Eurosup configuration. We also chose to keep the pressure waveform symetric. The amplitude h of the first shock is chosen equal to 0.6 and the signal energy is kept constant, so that the whole signal is entirely determined by a single parameter, the time interval Δt between the two first shocks (Fig. 19). This interval varies between 0 (the classic N wave) and 0.5 (25% of the total duration). Figure 20 shows the highest amplitude of the focused boom as a function of the interval between the two first shocks. Compared to an ''N'' wave, we first observe an amplitude decrease, the minimal value being reached for an interval between the two first shocks equal to 0.25 (12.5% of the total duration). The reduction of the amplitude is then about 20% compared to the N wave. For larger time intervals, the amplitude increases anew. This proves that potential ways for the reduction of a focused boom do exist. They require to produce incoming waves with multiple shock, both at the front *and* at the rear of the signal. The example of the Eurosup configuration shows that this objective should not be ruled out for a realistic configuration. Nevertheless, superboom reduction sonic remains a formidable challenge, especially for the rear part of the aircraft, which is especially complex from an aerodynamical point of view.

ACKNOWLEDGMENTS

Parts II, III, and IV of this investigation have been carried out under a contract awarded by the European Commission, Contract No. G4RD-CT-2000-00398. No part of this report may be used, reproduced and/or disclosed, in any form of by any means without the prior written permission of Université Pierre et Marie Curie and the SOBER project partners. 16/11/2001 All rights reserved.

Part V of this investigation was supported by Ministère de la Recherche (France), decisions No. 00 T0113 and 00 T0114.

Airy, G. B. (**1838**). ''On the intensity of light in the neighbourhood of a caustic,'' Trans. Cambridge Philos. Soc. **6**, 379–401.

Ames, W. F. (**1977**). *Numerical Methods for Partial Differential Equations* (Academic, New York), pp. 315–467.

Auger, T. (**2001**). ''Modélisation et simulation numérique de la focalisation d'ondes de choc acoustiques en milieu en mouvement. Application à la focalisation du bang sonique en accélération,'' thèse de l'Université Pierre et Marie Curie (Paris 6) (in French).
Auger, T., and Coulouvrat, F. (**2002**). ''Numerical simulation of sonic boom focusing,'' AIAA J. **40**, 1726–1734.
Berry, M. V. (**1976**). ''Waves and Thom's theorem,'' Adv. Phys. **25**, 1–26.
Blackstock, D. T., Hamilton, M. F., and Pierce, A. D. (**1998**). ''Progressive waves in lossless and lossy fluids,'' in *Nonlinear Acoustics* (Academic, San Diego), pp. 66–150.
Buchal, R. N., and Keller, J. B. (**1960**). ''Boundary layer problems in diffraction theory,'' Commun. Pure Appl. Math. **13**, 85–114.
Cambier, L. (**1999**). ''The elsA project,'' 1st ONERA/DLR Aerospace Symposium, Paris, 21–24 June 1999.
Cheng, H. K., and Hafez, M. M. (**2002**). ''The Superboom as a Tricomi problem: application,'' IUTAM Symposium Transsonicum IV, Göttingen (Germany), 2–6 September 2002 (proceedings to be published).
Coulouvrat, F. (**2000**). ''Focusing of weak acoustic shock waves at a caustic cusp,'' Wave Motion **32**, 233–245.
Coulouvrat, F. (**2002**). ''Sonic boom in the shadow zone: a geometrical theory of diffraction,'' J. Acoust. Soc. Am. **111**, 499–508.
Evans, T. P., and Doherty, J. J. (**1997**). ''The aerodynamic design of EUROSUP configuration,'' DERA/AS/ASD/CR97620/1.0.
Frøysa, K.-E., Tjøtta, J. N., and Berntsen, J. (**1993**). ''Finite amplitude effects in sound beams. Pure tone and pulsed excitation,'' in *Advances in Nonlinear Acoustics*, edited by H. Hobæk, 13th Int. Sym. Nonlinear Acoustics, Bergen, Norway, 28 June–2 July (World Scientific Singapore), pp. 233–238.
Gill, P. M., and Seebass, A. R. (**1973**). ''Nonlinear acoustic behavior at a caustic: an approximate analytical solution,'' AIAA Aeroacoustics Conference, Seattle (MIT, Cambridge), AIAA Paper 73-1037, pp. 353–386.
Guiraud, J.-P. (**1965**). ''Acoustique géométrique, bruit balistique des avions supersoniques et focalisation,'' J. Mec. **4**, 215–267 (in French).
Hayes, W. D. (**1968**). ''Similarity rules for nonlinear acoustic propagation through a caustic,'' Second Conference on Sonic Boom Research, NASA SP-180, pp. 165–171.
Hayes, W. D., Haefeli, R. C., and Kulsrud, H. E. (**1969**). ''Sonic boom propagation in a stratified atmosphere with computer program,'' NASA CR-1299.
Kravtsov, Y. A., and Orlov, Y. I. (**1993**). *Caustics, Catastrophes and Wave Fields* (Springer-Verlag, Berlin), pp. 8–33.
Landau, L. (**1945**). ''On shock waves at large distances from the place of their origin,'' J. Phys. U.S.S.R. **9**, 496–500.
Lee, Y. S., and Hamilton, M. F. (**1995**). ''Time-domain modeling of pulsed finite-amplitude sound beams,'' J. Acoust. Soc. Am. **97**, 906–917.
Marchiano, R., Thomas, J.-L., and Coulouvrat F. (**2003**). ''Experimental simulation of supersonic superboom in a water tank: nonlinear focusing of weak shock waves at a fold caustic,'' Phys. Rev. Lett. (to be published).
McDonald, B. E., and Ambrosiano, J. (**1984**). ''High order upwind flux methods for scalar hyperbolic conservation laws,'' J. Comput. Phys. **56**, 448–460.
Murman, E. M., and Cole, J. D. (**1971**). ''Calculation of plane steady transonic flows,'' AIAA J. **9**, 114–121.
Pestorius, F. M. (**1973**). ''Propagation of plane acoustic noise of finite amplitude,'' Technical Report ARL-TR-73-23 (Applied Research Laboratories, The University of Texas at Austin), AD778868.
Plotkin, K. J. (**2002**). ''State of the art of sonic boom modelling,'' J. Acoust. Soc. Am. **111**, 530–536.
Plotkin, K. J., and Page, J. A. (**2002**). ''Extrapolation of Sonic Boom Signatures from CFD Solutions,'' AIAA Pap. **2002-0922**, 1–6.
Seebass, A. R. (**1971**). ''Nonlinear acoustic behavior at a caustic,'' Third Conference on Sonic Boom Research, NASA SP-255, pp. 87–120.
Sturtevant, B., and Kulkarny, V. A. (**1976**). ''The focusing of weak shock waves,'' J. Fluid Mech. **73**, 651–671.
Thom, R. (**1972**). *Stabilité structurelle et morphogenèse* (Benjamin, Reading), pp. 72–107 (in French).
Wanner, J.-C., Vallée, J., Vivier, C., and Théry, C. (**1972**). ''Theoretical and experimental studies of the focus of sonic booms,'' J. Acoust. Soc. Am. **52**, 13–32.
Whitham, G. B. (**1952**). ''The flow pattern of a supersonic projectile,'' Commun. Pure Appl. Math. **5**, 301–348.
Zabolotskaya, E. A., and Khokhlov, R. V. (**1969**). ''Quasi-plane waves in the non-linear acoustics of confined beams,'' Sov. Phys. Acoust. **15**, 35–40.